

Honeycomb Lattice Iridates Na_2IrO_3 under Strong Spin-Orbit Interaction and Electron Correlation Studied by *Ab Initio* Scheme

Youhei Yamaji, Yusuke Nomura, Moyuru Kurita, Ryotaro Arita and Masatoshi Imada
Department of Applied Physics, University of Tokyo, Hongo, Bunkyo-ku, Tokyo, 113-8656, Japan.
(Dated: July 6, 2018)

An effective low-energy Hamiltonian of itinerant electrons for iridium oxide Na_2IrO_3 is derived by an *ab initio* downfolding scheme. The model is then reduced to an effective spin model on a honeycomb lattice by the strong coupling expansion. Here we show that the *ab initio* model contains spin-spin anisotropic exchange terms in addition to the extensively studied Kitaev and Heisenberg exchange interactions, and allows to describe the experimentally observed zigzag magnetic order, interpreted as the state stabilized by the antiferromagnetic coupling of the ferromagnetic chains. We clarify possible routes to realize quantum spin liquids from existing Na_2IrO_3 .

Introduction.— Cooperation and competition between strong electron correlations and spin-orbit couplings have recently attracted much attention. Iridium oxides offer playgrounds for such an interplay and indeed exhibit intriguing rich phenomena[1–4].

Especially, a theoretical prediction[1, 2] on the possible realization of quantum spin liquid state and Majorana fermion state proven by Kitaev [5] as the ground state of an exactly solvable model now called Kitaev model has inspired extensive studies on $A_2\text{IrO}_3$ ($A = \text{Na}$ or Li) as a model system to realize the Kitaev spin liquid. However, although Na_2IrO_3 is an insulator (presumably Mott insulator) with the optical gap ~ 0.35 eV[6], it was shown that Na_2IrO_3 does not show spin liquid properties experimentally but exhibits a zigzag type magnetic order [7, 8].

The Kitaev-Heisenberg model on the honeycomb lattice[1, 2, 9–11] was further proposed to describe Na_2IrO_3 , which includes isotropic superexchange couplings in addition to the Kitaev-type anisotropic nearest-neighbor Ising interactions whose anisotropy axes depend on the bond directions. However, it turned out that this model cannot be straightforwardly consistent with the zigzag order either. This discrepancy inspired further studies on suitable low-energy effective hamiltonians for $A_2\text{IrO}_3$ with $A = \text{Na}$ or Li . First, models with further neighbor couplings [7, 8, 12, 13] were studied. Additional Ising anisotropy[14] due to a strong trigonal distortion, which actually contradicts the distortions in the experiments [8] and in the *ab initio* treatments, was also examined. Quasimolecular orbitals[15], instead of the atomic orbitals assumed in the Kitaev-Hubbard model were claimed as a proper choice of the starting point. So far the origin of the zigzag type antiferromagnetic order observed for Na_2IrO_3 and the possible route to realize the quantum spin liquid are controversial.

In this Letter, we derive an *ab initio* spin model for Na_2IrO_3 and show that trigonal distortions present in Na_2IrO_3 in addition to the spin-orbit couplings holds the key: The simplest and realistic spin model for $A_2\text{IrO}_3$ will turn out to modify the Kitaev-Heisenberg hamiltonian by

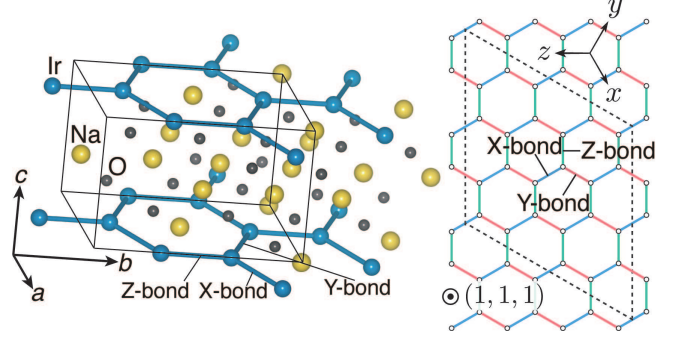


FIG. 1: (color online): Left panel: Crystal structure of Na_2IrO_3 . Right panel: Honeycomb lattice with X-, Y-, and Z-bonds. Same colored bonds indicate the same group. The x , y , and z axes in defining the t_{2g} -orbitals are illustrated as directions out of the honeycomb plane. The honeycomb plane is then perpendicular to $(x, y, z) = (1, 1, 1)$. The dashed boundary represents a 24-site cluster used later for the exact diagonalization.

additional anisotropic couplings as

$$\hat{H} = \sum_{\Gamma=X,Y,Z} \sum_{\langle \ell, m \rangle \in \Gamma} \vec{S}_{\ell}^T \mathcal{J}_{\Gamma} \vec{S}_m, \quad (1)$$

where $\vec{S}_{\ell}^T = (\hat{S}_{\ell}^x, \hat{S}_{\ell}^y, \hat{S}_{\ell}^z)$ is a vector of $\text{SU}(2)$ spin operators. The exchange couplings are given in matrices \mathcal{J}_{Γ} . The summations are over the nearest-neighbor pairs $\langle \ell, m \rangle$. The group of bond Γ with $\Gamma = X, Y$ and Z is defined in Fig. 1. The exchange matrices are parametrized as

$$\mathcal{J}_Z = \begin{bmatrix} J & I_1 & I_2 \\ I_1 & J & I_2 \\ I_2 & I_2 & K \end{bmatrix}, \mathcal{J}_X = \begin{bmatrix} K' & I_2'' & I_2' \\ I_2'' & J'' & I_1' \\ I_2' & I_1' & J' \end{bmatrix}, \quad (2)$$

$$\mathcal{J}_Y = \begin{bmatrix} J'' & I_2'' & I_1' \\ I_2'' & K' & I_2' \\ I_1' & I_2' & J' \end{bmatrix},$$

where we choose a real and symmetric parameterization by using $\text{U}(1)$ - and $\text{SU}(2)$ -symmetry of electron wave

functions and spin operators, respectively. The details of these exchange parameters are described in the following discussion.

In addition to the Kitaev coupling K and K' , and XY-type exchange J , magnetic anisotropy induced by a combination of spin-orbit couplings and trigonal distortions appears as anisotropic couplings such as I_1 and I_2 . These anisotropic couplings drastically change candidate quantum phases and competition among them in Na_2IrO_3 and related materials. With these extensions, we show that the model allows a realistic description of Na_2IrO_3 and provides a basis for further search of quantum spin liquids. To achieve quantitative accuracy, we include the anisotropic 2nd neighbor and 3rd neighbor couplings in our numerical calculations as detailed later.

Ab initio derivation and estimate of itinerant effective hamiltonian.— To discuss low-energy physics of Na_2IrO_3 , we employ a recently proposed multi-scale *ab initio* scheme for correlated electrons (MACE) [16]: First, we obtain the global band structure using the density functional theory (DFT). Second, using a Wannier projection on the Ir $5d$ t_{2g} target bands, we derive an effective model for the Ir $5d$ t_{2g} orbitals by the downfolding procedure taking into account the renormalization from the states other than the Ir $5d$ t_{2g} orbitals.

The global electronic structure was obtained by performing the density functional calculations using the Elk full-potential linearized augmented plane-wave code [17]. The muffin tin radii (R_{MT}) of 1.61, 2.14, and 1.55 bohr for Na, Ir and O were used, respectively. The maximum modulus for the reciprocal vectors K_{max} was chosen such that $R_{\text{MT}}^{\text{min}} K_{\text{max}} = 7.0$, where $R_{\text{MT}}^{\text{min}}$ is the smallest R_{MT} in the system. We employed the Perdew-Wang exchange-correlation functional [18].

We next constructed the Wannier orbitals from the Ir t_{2g} bands following the same procedure described in Ref. [19]. The derived xy -, yz -, zx -like orbitals satisfy the local cubic symmetry around the iridium atom. One body parameters $t_{\ell,m;a,b}^{\sigma,\sigma'}$ in the low-energy hamiltonian are given by the matrix elements of the Wannier orbitals as

$$t_{\ell,m;a,b}^{\sigma,\sigma'} = \int d\mathbf{r}_1 w_{\ell a \sigma}^*(\mathbf{r}_1) \hat{H}_{\text{KS}} w_{m b \sigma'}(\mathbf{r}_1) \quad (3)$$

with the Kohn-Sham hamiltonian \hat{H}_{KS} and the indices for sites ℓ and m , orbitals a and b , and spins σ and σ' .

The effective Coulomb interactions between these orbitals are estimated by the constrained random phase approximation (cRPA) [20]. Using the density response code for Elk [21], we obtain the charge susceptibility as

$$\chi(\mathbf{r}, \mathbf{r}', \omega) = \chi_0(\mathbf{r}, \mathbf{r}', \omega) + \int d\mathbf{r}_1 d\mathbf{r}_2 \chi_0(\mathbf{r}, \mathbf{r}_1, \omega) v(\mathbf{r}_1, \mathbf{r}_2) \chi(\mathbf{r}_2, \mathbf{r}', \omega),$$

where $v(\mathbf{r}_1, \mathbf{r}_2) = |\mathbf{r}_1 - \mathbf{r}_2|^{-1}$ is the bare Coulomb inter-

action.

$$\chi_0(\mathbf{r}, \mathbf{r}', \omega) = \sum_{j,j'}' \frac{(f_j - f_{j'}) \psi_{j'}(\mathbf{r}) \psi_{j'}^*(\mathbf{r}') \psi_j(\mathbf{r}') \psi_j^*(\mathbf{r})}{\omega - (\epsilon_{j'} - \epsilon_j) + i0^+}, \quad (4)$$

is the susceptibility of the noninteracting Kohn-Sham electrons. Here, ϵ_j and f_j are the energy and occupancy of the eigenstate ψ_j , and \sum' runs over all pairs of bands but excludes the cases where both j and j' belong to the target t_{2g} bands. We then calculate the partially-screened Coulomb interaction

$$W(\mathbf{r}, \mathbf{r}', \omega) = v(\mathbf{r}, \mathbf{r}') + \int d\mathbf{r}_1 d\mathbf{r}_2 v(\mathbf{r}, \mathbf{r}_1) \chi_0(\mathbf{r}_1, \mathbf{r}_2, \omega) W(\mathbf{r}_2, \mathbf{r}', \omega),$$

which yields the interaction parameters between the Wannier orbitals w as

$$U_{\mathcal{K}\mathcal{L}\mathcal{M}\mathcal{N}} = \lim_{\omega \rightarrow 0} \int d\mathbf{r}_1 d\mathbf{r}_2 w_{\mathcal{K}}^*(\mathbf{r}_1) w_{\mathcal{L}}^*(\mathbf{r}_2) W(\mathbf{r}_1, \mathbf{r}_2, \omega) \times w_{\mathcal{M}}(\mathbf{r}_1) w_{\mathcal{N}}(\mathbf{r}_2),$$

where $\mathcal{K}, \mathcal{L}, \mathcal{M}$, and \mathcal{N} are the combined indices for orbital and site. We took 100 unoccupied bands and $4 \times 4 \times 3$ \mathbf{k} and \mathbf{q} meshes, and the double Fourier transform of χ was done with the cutoff of $|\mathbf{G} + \mathbf{q}| = 5$ (1/a.u.) with \mathbf{G} being the reciprocal vector.

Ab initio model for t_{2g} hamiltonian— The derived multiband model consisting of t_{2g} -manifold of the iridium atoms is given by the t_{2g} -hamiltonian

$$\hat{H}_{t_{2g}} = \hat{H}_0 + \hat{H}_{\text{tri}} + \hat{H}_{\text{SOC}} + \hat{H}_U, \quad (5)$$

where each decomposed part is determined in the following: The hopping terms are given by

$$\hat{H}_0 = \sum_{\ell \neq m} \sum_{a,b=xy,yz,zx} \sum_{\sigma,\sigma'} t_{\ell,m;a,b}^{\sigma,\sigma'} \left[\hat{c}_{\ell a \sigma}^\dagger \hat{c}_{m b \sigma'} + \text{h.c.} \right]. \quad (6)$$

Here we note that, among all the hoppings, the dominant terms are the nearest-neighbor hopping $t \simeq t_{\ell,m;a,b}^{\sigma,\sigma} \simeq t_{\ell,m;b,a}^{\sigma,\sigma}$ that satisfies $(a, b) = (zx, xy)$, (xy, yz) , or (yz, zx) with $(\ell, m) \in X, Y$, and Z . This is consistent with the original proposal[1] for the Kitaev's compass-type exchange couplings.

The onsite atomic part is derived from Eq. (3) with $\ell = m$ and can be described as the contribution from the trigonal distortion (with orbital-dependent chemical potentials) and the atomic part of the spin-orbit coupling by introducing a vector representation $\vec{\hat{c}}_\ell^\dagger = (\hat{c}_{\ell yz \uparrow}^\dagger, \hat{c}_{\ell yz \downarrow}^\dagger, \hat{c}_{\ell zx \uparrow}^\dagger, \hat{c}_{\ell zx \downarrow}^\dagger, \hat{c}_{\ell xy \uparrow}^\dagger, \hat{c}_{\ell xy \downarrow}^\dagger)$ as

$$\hat{H}_{\text{tri}} = \sum_{\ell} \vec{\hat{c}}_\ell^\dagger \begin{bmatrix} -\mu_{yz} & \Delta & \Delta \\ \Delta & -\mu_{zx} & \Delta \\ \Delta & \Delta & -\mu_{xy} \end{bmatrix} \hat{\sigma}_0 \vec{\hat{c}}_\ell, \quad (7)$$

and

$$\hat{H}_{\text{SOC}} = \frac{\zeta_{\text{so}}}{2} \sum_{\ell} \hat{c}_{\ell}^{\dagger} \begin{bmatrix} 0 & +i\hat{\sigma}_z & -i\hat{\sigma}_y \\ -i\hat{\sigma}_z & 0 & +i\hat{\sigma}_x \\ +i\hat{\sigma}_y & -i\hat{\sigma}_x & 0 \end{bmatrix} \vec{c}_{\ell}. \quad (8)$$

Both the off-diagonal elements of the spin-independent part \hat{H}_{tri} and the spin-dependent part \hat{H}_{SOC} can be well described by a single parameter Δ and ζ_{so} , respectively. Due to the inherent crystal anisotropy, the chemical potential for the xy -orbitals, μ_{xy} , is different from μ_{yz} and μ_{zx} . The symmetry of these terms is slightly broken in the real crystal due to the stacking fault along the c -axis and the locations of other ions. However the deviation is much smaller than 0.05 eV.

The Coulomb term expressed by the Wannier orbital basis is well described by a symmetric form as

$$\begin{aligned} \hat{H}_U &= U \sum_{\ell} \sum_{a=yz,zx,xy} \hat{n}_{\ell a \uparrow} \hat{n}_{\ell a \downarrow} \\ &+ \sum_{\ell \neq m} \sum_{a,b} \frac{V_{\ell,m}}{2} (\hat{n}_{\ell a \uparrow} + \hat{n}_{\ell a \downarrow}) (\hat{n}_{m b \uparrow} + \hat{n}_{m b \downarrow}) \\ &+ \sum_{\ell} \sum_{a < b} \sum_{\sigma} [U' \hat{n}_{\ell a \sigma} \hat{n}_{\ell b \bar{\sigma}} + (U' - J_{\text{H}}) \hat{n}_{\ell a \sigma} \hat{n}_{\ell b \sigma}] \\ &+ J_{\text{H}} \sum_{\ell} \sum_{a \neq b} \left[\hat{c}_{\ell a \uparrow}^{\dagger} \hat{c}_{\ell b \downarrow}^{\dagger} \hat{c}_{\ell a \downarrow} \hat{c}_{\ell b \uparrow} + \hat{c}_{\ell a \uparrow}^{\dagger} \hat{c}_{\ell a \downarrow}^{\dagger} \hat{c}_{\ell b \downarrow} \hat{c}_{\ell b \uparrow} \right], \quad (9) \end{aligned}$$

with the local intra-orbital Coulomb repulsion, U , inter-orbital Coulomb repulsion, U' , the Hund's rule coupling, J_{H} , and the inter-atomic Coulomb repulsion, $V_{\ell,m}$. The orbital dependence of U , J_{H} and V are negligibly small.

The obtained tight binding parameters are given in Table I. We also list the orbital-averaged values of U , U' , J_{H} and V obtained by the cRPA. We note that $\Delta = -28$ meV for the t_{2g} model [22]. One might think that $\Delta = -28$ meV looks a tiny parameter. However it is crucial to keep it because it generates relevant anisotropy illustrated later in Fig.3.

Strong coupling limit, Minimal spin model for $A_2\text{IrO}_3$.— The *ab initio* parameters for the generalized Kitaev-Heisenberg model (1) are derived from t_{2g} hamiltonian $\hat{H}_{t_{2g}}$ in Eq.(5) by the second order perturbation theory: Here we take $\hat{H}_{\text{tri}} + \hat{H}_{\text{SOC}} + \hat{H}_U$ as an unperturbed hamiltonian and \hat{H}_0 as a perturbation. Since the ground state of $\hat{H}_{\text{tri}} + \hat{H}_{\text{SOC}} + \hat{H}_U$ is degenerate, we employ the standard degenerate perturbation theory. If we neglect Δ and μ_a ($a = yz, zx, xy$), the lowest Kramers doublets become so-called $J_{\text{eff}}=1/2$ states. The atomic ground state of an isolated iridium atom is preserved to be doublet irrespective of the amplitudes of Δ [23]. Then the generalized Kitaev-Heisenberg model describing pseudospin degrees of freedom is justified as an effective model in the ground state as well as at a finite temperature unless it exceeds both of Δ and ζ_{so} .

one-body			
t (eV)	$\mu_{xy} - \mu_{yz,zx}$ (eV)	ζ_{so} (eV)	Δ (eV)
0.27	0.035	0.39	-0.028
two-body			
U (eV)	U' (eV)	J_{H} (eV)	V (eV)
2.72	2.09	0.23	1.1

TABLE I: One-body and two-body parameters for $\hat{H}_{t_{2g}}$. The most relevant hopping parameter t , the atomic spin-orbit coupling ζ , and the trigonal distortion Δ , are shown for one-body part. Here, t is for $t_{\ell,m;\xi,\eta}^{\sigma,\sigma}$ for (ℓ, m) being the Z bond and its symmetric replacement for X and Y bonds. As for the two-body parameters, we list the cRPA results for the local intra-orbital Coulomb repulsion U , the Hund's rule coupling J_{H} , and the orbital-independent nearest-neighbor Coulomb repulsion V . Other small one-body parameters are given in Ref.23.

\mathcal{J}_Z (meV)	K	J	I_1	I_2		
	-30.7	4.4	-0.4	1.1		
$\mathcal{J}_{X,Y}$ (meV)	K'	J'	J''	I'_1	I'_2	I''_2
	-23.9	2.0	3.2	1.8	-8.4	-3.1

TABLE II: Nearest-neighbor exchange couplings derived by the strong coupling expansion from the *ab initio* t_{2g} model.

The exchange couplings \mathcal{J}_Z , \mathcal{J}_X , \mathcal{J}_Y , and further neighbor ones are derived through the second order perturbation theory by numerically diagonalizing the local part of the hamiltonian $\hat{H}_{\text{tri}} + \hat{H}_{\text{SOC}} + \hat{H}_U$ and by including all order terms with respect to ζ_{so} and Δ , irrespective of their amplitudes. (See Supplemental Material.) Thus obtained *ab initio* values for Na_2IrO_3 are given in Table II. We remark that $K \sim -30.1$ meV is negative and $J \sim 4.4$ meV is positive for the Z -bonds. For numerical calculations, we also include the 2nd and 3rd neighbor couplings for more accurate *ab initio* calculations [23].

The model (1) with the *ab initio* parameters in Table II together with small and detailed 2nd and 3rd exchange couplings[23] was solved by the exact diagonalization for a 24-site cluster. We also calculate finite temperature properties for the cluster by using the thermal pure quantum states[24], which offers an algorithm similar to the finite-temperature Lanczos[25] and earlier works[26]. They well reproduce the experimentally observed zigzag magnetic order as the ground state and finite temperature properties. See detailed results in later discussions for Fig.2 and Supplemental Material.

Neither large further neighbor exchange couplings [7, 8, 12, 13] nor antiferromagnetic Kitaev couplings $K > 0$ [2, 27] assumed and required to reproduce the experimental zigzag magnetic order in the literature are realistic in the *ab initio* point of view. In addition, the amplitudes of the anisotropic couplings I_1 and I_2 comparable with J are crucially important to reproduce the experimental

results, contrary to the assumptions in Refs. 2 and 27.

The stabilization of the zigzag order is interpreted as follows: If we assume the magnetic ordered moment along $(x, y, z) = (1, 1, 0)$, the zigzag order is interpreted as ferromagnetically-ordered chains consisting of the X - and Y -bonds (stabilized by K' and I_2''), antiferromagnetically coupled each other by the Z -bonds with J , which is in contrast to a quantum-chemistry estimate that neglects I_2 , I_2' , and I_2'' [28]. The alignment along $(1, 1, 0)$ assumed here indeed agrees with the result of the pinning field analysis[23] shown in Fig.2(a). It is also confirmed by the nearest-neighbor spin-spin correlations, $\langle \hat{S}_\ell^x \hat{S}_m^x \rangle = \langle \hat{S}_\ell^y \hat{S}_m^y \rangle = -0.021$, $\langle \hat{S}_\ell^z \hat{S}_m^z \rangle = 0.128$, for Z -bond, and $\langle \hat{S}_\ell^x \hat{S}_m^x \rangle = 0.052(0.098)$, $\langle \hat{S}_\ell^y \hat{S}_m^y \rangle = 0.098(0.052)$, $\langle \hat{S}_\ell^z \hat{S}_m^z \rangle = -0.020$, for X -bond(Y -bond).

Comparison with experiments— Our effective spin model reproduces not only the zigzag order but magnetic specific heats and anisotropic uniform magnetic susceptibilities consistently with experiments, as shown in Fig.2(b) and (c). For the specific heats, our results are consistent without adjustable parameters. The uniform magnetic susceptibilities χ show Curie-Weiss behaviors and $\chi_{ab} < \chi_c$, where χ_{ab} (χ_c) is the inplane (out-of-plane) susceptibility, which are consistent with experiments. If we introduce a g -factor, $g = 1.5$, and anisotropic van Vleck term, $\chi_0 = 1 \times 10^{-4} \text{cm}^3/\text{mol}$ for χ_c , high-temperature behaviors of χ are qualitatively reproduced as shown in Fig.2(c). Here we note that the electron's spin moments are different from those of the effective spin models depending on the choice of the Kramers doublets, $|\uparrow\rangle$ and $|\downarrow\rangle$ [23].

Phase diagram in lattices distorted from Na_2IrO_3 Now we examine the sensitivity of the ground state for the *ab initio* parameter of Na_2IrO_3 to perturbations and search candidates of other quantum states possibly induced by a thermodynamic control such as pressure or in derivatives of Na_2IrO_3 such as $\text{Na}_{2-x}\text{Li}_x\text{IrO}_3$. Here we choose the trigonal distortion Δ as an experimentally accessible control parameter. First, the Δ -dependence of the exchange couplings is illustrated in Fig.3(a). The ground state of the generalized Kitaev-Heisenberg model is shown in Fig.3(b) when the trigonal distortion Δ is taken as a control parameter.

How to approach spin liquids.— As already evident in Table.II, the *ab initio* effective spin model for Na_2IrO_3 is governed by dominant Kitaev-type ferromagnetic exchange couplings. By expanding the lattice, the spin liquid phase may become accessible: Expansion of the lattice makes the hopping parameters other than the dominant one t negligible. In addition, the environment of the iridium atoms approach the spherical limit where the intra-orbital Coulomb repulsion U' satisfies $U' = U - 2J_H$. Indeed, when we omit the hopping parameters other than t and increase J_H up to 0.3 eV to satisfy

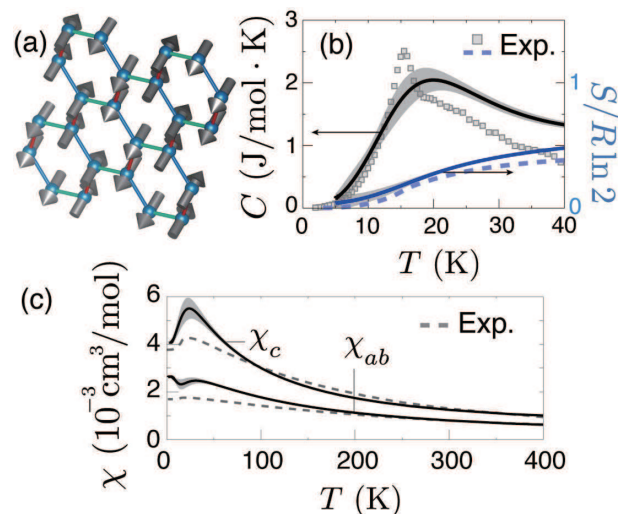


FIG. 2: (color online): Ground state and finite temperature properties of the generalized Kitaev-Heisenberg model for Na_2IrO_3 calculated for the 24-site cluster by using the Lanczos method and thermal pure quantum states[24]. (a) Ground state magnetic order determined by applying tiny local magnetic fields ($\sim 10^{-2}$ meV) at a single site. (b) Temperature-dependence of specific heat C and entropy S , which are consistent with an experiment[29]. Shaded area shows uncertainty due to finite size effects[24]. (c) Temperature-dependence of inplane and out-of-plane magnetic susceptibilities, which are also consistent with the experiment[29] at high temperatures.

$U' = U - 2J_H$, we obtain the spin liquid states adiabatically connected to the Kitaev's spin liquid as shown in Fig.3(c).

Summary. We have shown that the realistic parameter of the *ab initio* model for Na_2IrO_3 reproduces the experimentally observed robust zigzag magnetic order, while a quantum spin liquid phase adiabatically connected to the Kitaev spin liquid emerges when the smaller trigonal distortion Δ and expanded lattice constants are satisfied. In this sense, uniaxial strain to reduce Δ is helpful as an approach to realize the spin liquids. Clearly further studies are needed: More accurate estimate of the phase diagram of the generalized Kitaev-Heisenberg model is certainly helpful. More detailed studies by taking account of full quantum fluctuations and the effects of realistic itinerancy beyond the strong coupling limit are future intriguing issues.

Y. N. is supported by the Grant-in-Aid for JSPS Fellows (Grant No.12J08652). M. K. is supported by Grant-in-Aid for JSPS Fellows (Grant No.12J07338). R. A. is supported by Funding Program for World-Leading Innovative R&D on Science and Technology (FIRST program) on "Quantum Science on Strong Correlation." This work is financially supported by MEXT HPCI Strategic Programs for Innovative Research (SPIRE) (hp130007) and Computational Materials Science Initiative (CMSI). Numerical calculation was partly carried out at the Su-

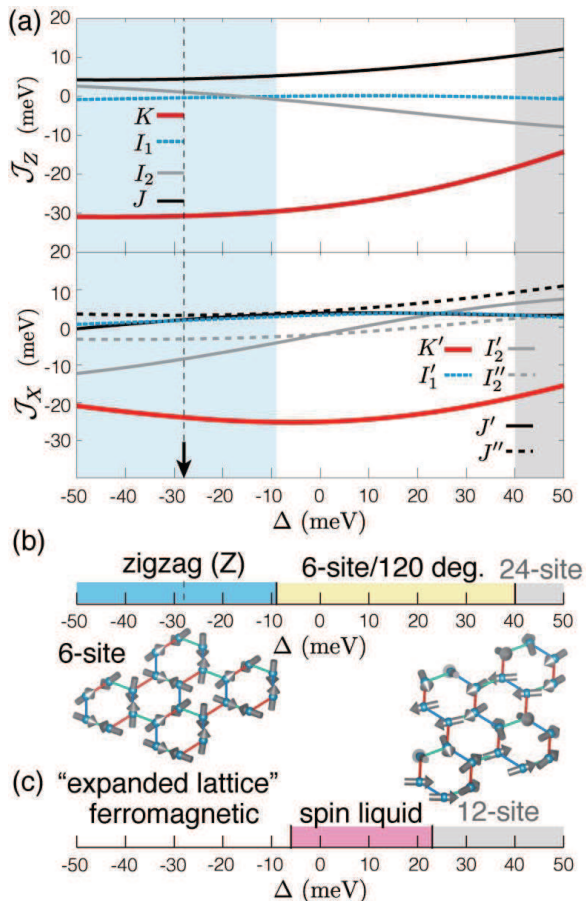


FIG. 3: (color online): (a) Δ -dependence of matrix elements of \mathcal{J}_Z , \mathcal{J}_X as functions of Δ . Around the *ab initio* values at Δ (~ -28 meV) listed in Table II, $K < 0$, $K' < 0$, $J > 0$, $J' > 0$, and $J'' > 0$ are stably satisfied with gradual dependences on Δ . (b) Ground state phase diagram for Na_2IrO_3 with lattice distortions represented by changes in Δ . The phase boundaries are determined by anomalies in second derivatives of the exact energy for the 24-site cluster with respect to Δ . Around the *ab initio* parameter $\Delta = -28$ meV, the zigzag order appears. By increasing Δ , a 6-site unit cell order (or 120° -structure[27]) illustrated in the lower left panel and a 24-site unit cell long-period order[23], appear. (c) Δ -dependence of the ground state of the generalized Kitaev-Heisenberg model for “expanded lattices.” Here we neglect the small hopping parameters other than t and take a larger Hund coupling $J_H = 0.3$ eV. Spin liquid phases compete with ferromagnetic states and 12-site unit cell orders illustrated in the lower right panel[23].

percomputer Center, Institute for Solid State Physics, Univ. of Tokyo. This work was also supported by Grant-in-Aid for Scientific Research (No. 22104010, and No. 223400901) from MEXT, Japan.

- [1] G. Jackeli and G. Khaliullin, Phys. Rev. Lett. **102**, 017205 (2009).
- [2] J. Chaloupka, G. Jackeli, and G. Khaliullin, Phys. Rev. Lett. **105**, 027204 (2010).
- [3] X. Wan, A. M. Turner, A. Vishwanath, and S. Y. Savrasov, Phys. Rev. B **83**, 205101 (2011).
- [4] W. Witczak-Krempa, C. Gang, Y.-B. Kim, and L. Balents, arXiv:1305.2193.
- [5] A. Kitaev, Annals Phys. **321**, 2 (2006).
- [6] R. Comin, G. Levy, B. Ludbrook, Z.-H. Zhu, C. Veenstra, J. Rosen, Y. Singh, P. Gegenwart, D. Stricker, J. Hancock, et al., Phys. Rev. Lett. **109**, 266406 (2012).
- [7] S. K. Choi, R. Coldea, A. N. Kolmogorov, T. Lancaster, I. I. Mazin, S. J. Blundell, P. G. Radaelli, Y. Singh, P. Gegenwart, K. R. Choi, et al., Phys. Rev. Lett. **108**, 127204 (2012).
- [8] F. Ye, S. Chi, H. Cao, B. C. Chakoumakos, J. A. Fernandez-Baca, R. Custelcean, T. F. Qi, O. B. Korneta, and G. Cao, Phys. Rev. B **85**, 180403 (2012).
- [9] Y. Singh, S. Manni, J. Reuther, T. Berlijn, R. Thomale, W. Ku, S. Trebst, and P. Gegenwart, Phys. Rev. Lett. **108**, 127203 (2012).
- [10] J. Reuther, R. Thomale, and S. Trebst, Phys. Rev. B **84**, 100406 (2011).
- [11] J. Chaloupka, G. Jackeli, and G. Khaliullin, Phys. Rev. Lett. **110**, 097204 (2013).
- [12] I. Kimchi and Y.-Z. You, Phys. Rev. B **84**, 180407 (2011).
- [13] A. F. Albuquerque, D. Schwandt, B. Hetényi, S. Capponi, M. Mambrini, and A. M. Läuchli, Phys. Rev. B **84**, 024406 (2011).
- [14] S. Bhattacharjee, S.-S. Lee, and Y. B. Kim, New Journal of Physics **14**, 073015 (2012).
- [15] I. I. Mazin, H. O. Jeschke, K. Foyevtsova, R. Valentí, and D. I. Khomskii, Phys. Rev. Lett. **109**, 197201 (2012).
- [16] T. Miyake and M. Imada, J. Phys. Soc. Jpn. **79**, 112001 (2010).
- [17] <http://elk.soruceforge.net/>.
- [18] J. P. Perdew and Y. Wang, Phys. Rev. B **45**, 13244 (1992).
- [19] R. Arita, J. Kuneš, A. V. Kozhevnikov, A. G. Eguiluz, and M. Imada, Phys. Rev. Lett. **108**, 086403 (2012).
- [20] F. Aryasetiawan, M. Imada, A. Georges, K. Gabriel, S. Biermann, and A. I. Lichtenstein, Phys. Rev. B **70**, 195104 (2004).
- [21] A. Kozhevnikov, A. Eguiluz, and T. Schulthess, SC'10 Proceedings of the 2010 ACM/IEEE International Conference for High Performance Computing, Networking, Storage, and Analysis p. 1 (2010).
- [22] The small amplitude of the trigonal distortion $\Delta = -28$ meV is different from the previous result[30]. Here we note that differences between Ref.30 and ours: First, the electronic band structure around the Fermi level in Ref.20 is different from the result in Ref.15 and ours. In addition, in Ref.30, the tight-binding parameter of a dp -hamiltonian is obtained through numerically fitting the LDA dispersion with notable fitting errors, while we construct the model by directly calculating the hopping matrix elements with the t_{2g} Wannier orbitals.
- [23] See Supplemental Materials.
- [24] S. Sugiura and A. Shimizu, Phys. Rev. Lett. **108**, 240401 (2012).

- [25] J. Jaklič and P. Prelovšek, Phys. Rev. B **49**, 5065 (1994).
 [26] M. Imada and M. Takahashi, J. Phys. Soc. Jpn. **55**, 3354 (1986).
 [27] J. Rau, E. K.-H. Lee, and H.-Y. Kee, arXiv:1310.7940.
 [28] V. K. Katukuri, S. Nishimoto, V. Yushankhai, A. Stoyanova, H. Kandpal, C. Sungkyun, R. Coldea, I. Rousochatzakis, L. Hozoi, and J. van den Brink, arXiv:1312.7437.
 [29] Y. Singh and P. Gegenwart, Phys. Rev. B **82**, 064412 (2010).
 [30] C. H. Kim, H. S. Kim, H. Jeong, H. Jin, and J. Yu, Phys. Rev. Lett. **108**, 106401 (2012).

Supplemental Materials

ATOMIC GROUND STATE OF AN ISOLATED IRIDIUM ATOM

The eigenstates of the t_{2g} -shell of an isolated iridium ion Ir^{+4} is described by the local hamiltonian $\hat{H}_{\text{tri}} + \hat{H}_{\text{SOC}} + \hat{H}_U$. For any amplitude of the trigonal distortion Δ , the atomic ground state with 5 electrons in the t_{2g} -shell is a doublet, as shown in Fig.4. The excitation gap among the ground state doublet and the excited doublet (or quartet for $\Delta = 0$) is always larger than $\zeta_{\text{so}} = 0.39$ eV. Therefore, the present pseudo-spin model derived in the main article remains valid at temperatures roughly lower than $\zeta_{\text{so}}/k_B \simeq 4 \times 10^3$ K.

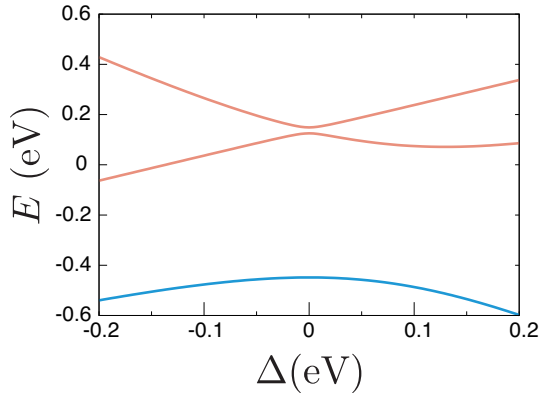


FIG. 4: Three doublet eigenstates of the local hamiltonian $\hat{H}_{\text{tri}} + \hat{H}_{\text{SOC}}$ with 5 electrons in the t_{2g} -shell as functions of the trigonal distortion Δ . The Coulomb term \hat{H}_U causes a constant shift in these three doublets. The doublet ground state is shown in the blue curve, while the red curves represent the excited doublet states.

Due to the trigonal distortion, $\text{SU}(2)$ rotation and $\text{U}(1)$ gauge transformation of electron wave functions for the Kramers doublet change the matrix elements of \mathcal{J}_Γ ($\Gamma = X, Y, Z$), \mathcal{J}_2 , and \mathcal{J}_3 , where, for further neighbor exchange couplings \mathcal{J}_2 , and \mathcal{J}_3 , details are given in the

following section. In the present Letter, we choose a Kramers doublet $|\uparrow\rangle$ and $|\downarrow\rangle$ as

$$\begin{aligned}
 |\uparrow\rangle = & z_1 \hat{c}_{yz\downarrow}^\dagger \hat{c}_{zx\uparrow}^\dagger \hat{c}_{zx\downarrow}^\dagger \hat{c}_{xy\uparrow}^\dagger \hat{c}_{xy\downarrow}^\dagger |0\rangle \\
 & + z_2 \hat{c}_{yz\uparrow}^\dagger \hat{c}_{zx\uparrow}^\dagger \hat{c}_{zx\downarrow}^\dagger \hat{c}_{xy\uparrow}^\dagger \hat{c}_{xy\downarrow}^\dagger |0\rangle \\
 & + z_1^* \hat{c}_{yz\uparrow}^\dagger \hat{c}_{yz\downarrow}^\dagger \hat{c}_{zx\downarrow}^\dagger \hat{c}_{xy\uparrow}^\dagger \hat{c}_{xy\downarrow}^\dagger |0\rangle \\
 & - iz_2 \hat{c}_{yz\uparrow}^\dagger \hat{c}_{yz\downarrow}^\dagger \hat{c}_{zx\uparrow}^\dagger \hat{c}_{zx\downarrow}^\dagger \hat{c}_{xy\downarrow}^\dagger |0\rangle \\
 & - h \hat{c}_{yz\uparrow}^\dagger \hat{c}_{yz\downarrow}^\dagger \hat{c}_{zx\uparrow}^\dagger \hat{c}_{zx\downarrow}^\dagger \hat{c}_{xy\downarrow}^\dagger |0\rangle \\
 & + e^{-i\pi/4} f \hat{c}_{yz\uparrow}^\dagger \hat{c}_{yz\downarrow}^\dagger \hat{c}_{zx\uparrow}^\dagger \hat{c}_{zx\downarrow}^\dagger \hat{c}_{xy\downarrow}^\dagger |0\rangle, \quad (10)
 \end{aligned}$$

and

$$\begin{aligned}
 |\downarrow\rangle = & -z_2^* \hat{c}_{yz\downarrow}^\dagger \hat{c}_{zx\uparrow}^\dagger \hat{c}_{zx\downarrow}^\dagger \hat{c}_{xy\uparrow}^\dagger \hat{c}_{xy\downarrow}^\dagger |0\rangle \\
 & + z_1^* \hat{c}_{yz\uparrow}^\dagger \hat{c}_{zx\uparrow}^\dagger \hat{c}_{zx\downarrow}^\dagger \hat{c}_{xy\uparrow}^\dagger \hat{c}_{xy\downarrow}^\dagger |0\rangle \\
 & - iz_2^* \hat{c}_{yz\uparrow}^\dagger \hat{c}_{yz\downarrow}^\dagger \hat{c}_{zx\downarrow}^\dagger \hat{c}_{xy\uparrow}^\dagger \hat{c}_{xy\downarrow}^\dagger |0\rangle \\
 & + z_1 \hat{c}_{yz\uparrow}^\dagger \hat{c}_{yz\downarrow}^\dagger \hat{c}_{zx\uparrow}^\dagger \hat{c}_{zx\downarrow}^\dagger \hat{c}_{xy\downarrow}^\dagger |0\rangle \\
 & - e^{+i\pi/4} f \hat{c}_{yz\uparrow}^\dagger \hat{c}_{yz\downarrow}^\dagger \hat{c}_{zx\uparrow}^\dagger \hat{c}_{zx\downarrow}^\dagger \hat{c}_{xy\downarrow}^\dagger |0\rangle \\
 & - h \hat{c}_{yz\uparrow}^\dagger \hat{c}_{yz\downarrow}^\dagger \hat{c}_{zx\uparrow}^\dagger \hat{c}_{zx\downarrow}^\dagger \hat{c}_{xy\downarrow}^\dagger |0\rangle, \quad (11)
 \end{aligned}$$

where z_1 , z_2 , f and h are coefficients of the linear combinations. In the above parameterization of the Kramers doublets, the $J_{\text{eff}} = 1/2$ -state is represented by taking the coefficients $z_1 = (1-i)/\sqrt{6}$, $z_2 = h = 0$, and $f = 1/\sqrt{6}$. Our choice for the above Kramers doublet give us real number elements in the nearest-neighbor exchange coupling along the Z -bond, \mathcal{J}_Z .

For the *ab initio* model, we choose the parameter set (z_1, z_2, f, h) that diagonalizes the z -component of the reduced spin operators for the t_{2g} -manifold defined as

$$\left[\tilde{S}_{\text{tot}}^\alpha \right]_{\sigma\sigma'} = \langle \sigma | \sum_a \sum_{\sigma'} \hat{c}_{a\sigma}^\dagger \hat{\sigma}^\alpha \hat{c}_{a\sigma'} / 2 | \sigma' \rangle, \quad (12)$$

where $\alpha = x, y, z$. By using the resultant Kramers doublet, the total magnetic moment consisting of the reduced spin and angular momentum operators, $\tilde{S}_{\text{tot}}^\alpha$ and $\tilde{L}_{\text{tot}}^\alpha$, for the t_{2g} -manifold is expressed by the $\text{SU}(2)$ operators \hat{S}^α . For the *ab initio* model, the total magnetic moment is given as

$$\begin{bmatrix} 2\tilde{S}_{\text{tot}}^x - \tilde{L}_{\text{tot}}^x \\ 2\tilde{S}_{\text{tot}}^y - \tilde{L}_{\text{tot}}^y \\ 2\tilde{S}_{\text{tot}}^z - \tilde{L}_{\text{tot}}^z \end{bmatrix} = 2 \begin{bmatrix} -0.07 & +0.94 & -0.24 \\ +0.94 & -0.07 & +0.24 \\ -0.07 & +0.07 & +1.07 \end{bmatrix} \begin{bmatrix} \hat{S}^x \\ \hat{S}^y \\ \hat{S}^z \end{bmatrix} \quad (13)$$

FURTHER NEIGHBOR EXCHANGE COUPLINGS AND DETAILS OF THE HOPPING PARAMETERS

For quantitative accuracy, we include dominant 2nd and 3rd neighbor exchange couplings represented by \hat{H}'

\mathcal{J}_2 (meV)	$K^{(2nd)}$	$J^{(2nd)}$	$I_1^{(2nd)}$	$I_2^{(2nd)}$
	-1.2	-0.8	1.0	-1.4
\mathcal{J}_3 (meV)	$J^{(3rd)}$			
	1.7			

TABLE III: Second and third neighbor exchange couplings derived by the strong coupling expansion from the *ab initio* t_{2g} model.

for our numerical calculations:

$$\hat{H}' = \sum_{\langle \ell, m \rangle' \in Z_{2nd}} \vec{S}_\ell^T \mathcal{J}_2 \vec{S}_m + \sum_{\langle \ell, m \rangle''} \vec{S}_\ell^T \mathcal{J}_3 \vec{S}_m, \quad (14)$$

where further exchange couplings are given in matrices \mathcal{J}_2 , and \mathcal{J}_3 . The summations are over the second neighbor pairs $\langle \ell, m \rangle'$, and the third neighbor pairs $\langle \ell, m \rangle''$. For the 2nd neighbor pairs, exchange couplings are finite if they belong to the group of 2nd neighbor bonds perpendicular to the Z -bond, Z_{2nd} . These exchange matrices are parametrized as

$$\mathcal{J}_2 = \begin{bmatrix} J^{(2nd)} & I_1^{(2nd)} & I_2^{(2nd)} \\ I_1^{(2nd)} & J^{(2nd)} & I_2^{(2nd)} \\ I_2^{(2nd)} & I_2^{(2nd)} & K^{(2nd)} \end{bmatrix}, \quad (15)$$

and

$$\mathcal{J}_3 = \begin{bmatrix} J^{(3rd)} & 0 & 0 \\ 0 & J^{(3rd)} & 0 \\ 0 & 0 & J^{(3rd)} \end{bmatrix}, \quad (16)$$

where the obtained parameters are given in Table III. The all of the matrix elements of the 2nd and 3rd neighbor exchange couplings for other bonds, Dzyaloshinskii-Moriya-type couplings, as well as the couplings for even further neighbor bonds are smaller than 1 meV and neglected.

For derivation of these exchange parameters, we use detailed *ab initio* hopping parameters summarized in Table IV.

SECOND ORDER PERTURBATION

In the present Letter, we derive a generalized Kitaev-Heisenberg model by employing second-order degenerated perturbation theory from a strong coupling limit: We perform the perturbation by taking $\hat{H}_{\text{tri}} + \hat{H}_{\text{SOC}} + \hat{H}_U$ as the unperturbed hamiltonian and \hat{H}_0 as the perturbation.

As clarified in the above section, the ground state of the local part of the unperturbed hamiltonian $\hat{H}_{\text{tri}} + \hat{H}_{\text{SOC}} + \hat{H}_U$ is a Kramers doublet, but, strictly speaking, it deviates from the so-called $J_{\text{eff}} = 1/2$ state if $\Delta \neq 0$. We assign pseudo-spin degree of freedom to this doublet.

Z	$yz \uparrow$	$yz \downarrow$	$zx \uparrow$	$zx \downarrow$	$xy \uparrow$	$xy \downarrow$
$yz \uparrow$	31+0i	0+0i	273+8i	4+4i	-16-2i	10+39i
$yz \downarrow$	0+0i	31+0i	-4+4i	273-8i	-10+39i	-16+2i
$zx \uparrow$	273-8i	-4-4i	31+0i	0+0i	-16+2i	-39-10i
$zx \downarrow$	4-4i	273+8i	0+0i	31+0i	39-10i	-16-2i
$xy \uparrow$	-16+2i	-10-39i	-16-2i	39+10i	43+0i	0+0i
$xy \downarrow$	10-39i	-16-2i	-39+10i	-16+2i	0+0i	43+0i
X	$yz \uparrow$	$yz \downarrow$	$zx \uparrow$	$zx \downarrow$	$xy \uparrow$	$xy \downarrow$
$yz \uparrow$	-7+0i	0+0i	-18-11i	-36+3i	-25+39i	11-2i
$yz \downarrow$	0+0i	-7+0i	36+3i	-18+11i	-11-2i	-25-39i
$zx \uparrow$	-18+11i	36-3i	36+0i	0+0i	276+5i	5+8i
$zx \downarrow$	-36-3i	-18-11i	0+0i	36+0i	-5+8i	276-5i
$xy \uparrow$	-25-39i	-11+2i	276-5i	-5-8i	38+0i	0+0i
$xy \downarrow$	11+2i	-25+39i	5-8i	276+5i	0+0i	38+0i
Z_{2nd}	$yz \uparrow$	$yz \downarrow$	$zx \uparrow$	$zx \downarrow$	$xy \uparrow$	$xy \downarrow$
$yz \uparrow$	0-3i	0+4i	-85+0i	-2-2i	12-2i	-1+9i
$yz \downarrow$	0+4i	0+3i	2-2i	-85+0i	1+9i	12+2i
$zx \uparrow$	-30+1i	-2-2i	0-3i	4+0i	-20+3i	-10+0i
$zx \downarrow$	2-2i	-30-1i	-4+0i	0+3i	10+0i	-20-3i
$xy \uparrow$	-20+3i	0-10i	12-2i	9-1i	-2+6i	0+0i
$xy \downarrow$	0-10i	-20-3i	-9-1i	12+2i	0+0i	-2-6i
Z_{3rd}	$yz \uparrow$	$yz \downarrow$	$zx \uparrow$	$zx \downarrow$	$xy \uparrow$	$xy \downarrow$
$yz \uparrow$	-10+0i	0+0i	-13+0i	-1-1i	18+0i	0+4i
$yz \downarrow$	0+0i	-10+0i	1-1i	-13+0i	0+4i	18+0i
$zx \uparrow$	-13+0i	1+1i	-10+0i	0+0i	18+0i	-4+0i
$zx \downarrow$	-1+1i	-13+0i	0+0i	-10+0i	4+0i	18+0i
$xy \uparrow$	18+0i	0-4i	18+0i	4+0i	-37+0i	0+0i
$xy \downarrow$	0-4i	18+0i	-4+0i	18+0i	0+0i	-37+0i

TABLE IV: Detailed hopping parameters for nearest-, 2nd, and 3rd neighbor pairs of the iridium sites. The unit of the hopping parameters is given by meV. For the nearest-neighbor hoppings, the hoppings along the Z -bond and X -bond are shown, where the hoppings along the Y -bond is obtained by exchanging indices in the hoppings along the X -bond. The directions of these hopping processes are illustrated in Fig.6(a) later.

For illustrative purpose, we focus on a set of nearest-neighbor sites, the ℓ -th and m -th sites. Then we calculate the perturbation energy through the second order processes as

$$E_{\sigma_1, \sigma_2; \sigma_3, \sigma_4}^{(2)} = \langle m\sigma_2 | \langle \ell\sigma_1 | \hat{H}_0 \sum_n \frac{|n\rangle \langle n|}{E_n - E_0} \hat{H}_0 | \ell\sigma_3 \rangle | m\sigma_4 \rangle, \quad (17)$$

where $\sigma_j = \uparrow, \downarrow$ ($j = 1, 2, 3, 4$) is a pseudo-spin index, and $|n\rangle$ is an intermediate eigenstate of $\hat{H}_{\text{tri}} + \hat{H}_{\text{SOC}} + \hat{H}_U$ with 4 and 6 electrons at the ℓ -th and m -th site, respectively, or 6 and 4 electrons at the ℓ -th and m -th site, respectively. Here E_0 is the ground-state energy of the two sites with 5 electrons per site and E_n is an energy eigenvalues of an intermediate state of the two sites. The eigenstates $|n\rangle$ and eigenvalues E_n are obtained by numerically diagonalizing $\hat{H}_{\text{tri}} + \hat{H}_{\text{SOC}} + \hat{H}_U$.

From the perturbation energy $E_{\sigma_1, \sigma_2; \sigma_3, \sigma_4}^{(2)}$, we obtain the exchange couplings as follows. If we assume the bond

zigzag (Z)	6-site/120°	24-site	12-site
(0, 1)	(1/3, 1)	(1/6, 1/2)	(1/3, 0)

TABLE V: List of the momenta at which the dominant peaks appear in the magnetic structure factors calculated for each magnetic ordered phases in the phase diagrams, Fig.3(b) and (c) of the main article. Momenta are defined in a two dimensional Brillouin zone that is used in Ref.7 of the main article and Fig.6(b).

connecting the ℓ -th and m -th sites is a Z-bond, the exchange couplings are given for the minimal spin model for $A_2\text{IrO}_3$ as

$$K = +2 \left[E_{\sigma,\sigma;\sigma,\sigma}^{(2)} - E_{\sigma,\bar{\sigma};\sigma,\bar{\sigma}}^{(2)} \right], \quad (18)$$

$$J = +2E_{\sigma,\bar{\sigma};\bar{\sigma},\sigma}^{(2)}, \quad (19)$$

$$I_1 = -2\text{Im} \left\{ E_{\uparrow,\uparrow;\downarrow,\downarrow}^{(2)} \right\} = +2\text{Im} \left\{ E_{\downarrow,\downarrow;\uparrow,\uparrow}^{(2)} \right\}, \quad (20)$$

$$\begin{aligned} I_2 &= +4\text{Re} \left\{ E_{\uparrow,\uparrow;\downarrow,\downarrow}^{(2)} \right\} = -4\text{Im} \left\{ E_{\uparrow,\uparrow;\downarrow,\downarrow}^{(2)} \right\} \\ &= +4\text{Re} \left\{ E_{\uparrow,\uparrow;\uparrow,\uparrow}^{(2)} \right\} = -4\text{Im} \left\{ E_{\uparrow,\uparrow;\uparrow,\uparrow}^{(2)} \right\} \\ &= -4\text{Re} \left\{ E_{\downarrow,\downarrow;\uparrow,\downarrow}^{(2)} \right\} = -4\text{Im} \left\{ E_{\downarrow,\downarrow;\uparrow,\downarrow}^{(2)} \right\} \\ &= -4\text{Re} \left\{ E_{\downarrow,\downarrow;\downarrow,\uparrow}^{(2)} \right\} = -4\text{Im} \left\{ E_{\downarrow,\downarrow;\downarrow,\uparrow}^{(2)} \right\}. \end{aligned} \quad (21)$$

For the 2nd and 3rd neighbor bond, the matrix elements of the exchange couplings \mathcal{J}_2 and \mathcal{J}_3 as functions of the trigonal distortion Δ are calculated by the 2nd order perturbation as shown in Fig.5.

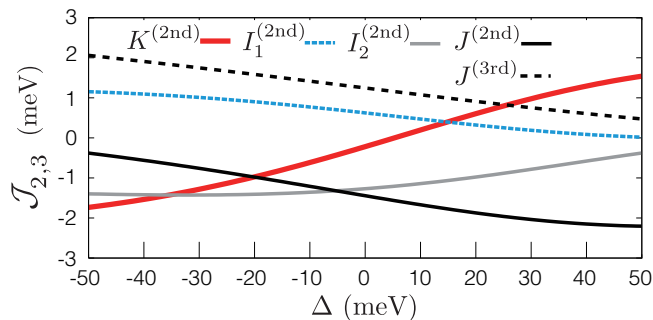


FIG. 5: Exchange couplings for 2nd and 3rd neighbor bond as functions of Δ .

MAGNETIC BRAGG PEAKS AND PINNING FIELD ANALYSIS

Peaks in spin structure factors, which may correspond to the magnetic Bragg peaks in the thermodynamic limit,

are primarily used to determine magnetic orders in the exact diagonalization. The 2D unit cell in the honeycomb layer of Na_2IrO_3 and the peaks of the spin structure factors are shown in Fig.3. In Table V, the magnetic Bragg

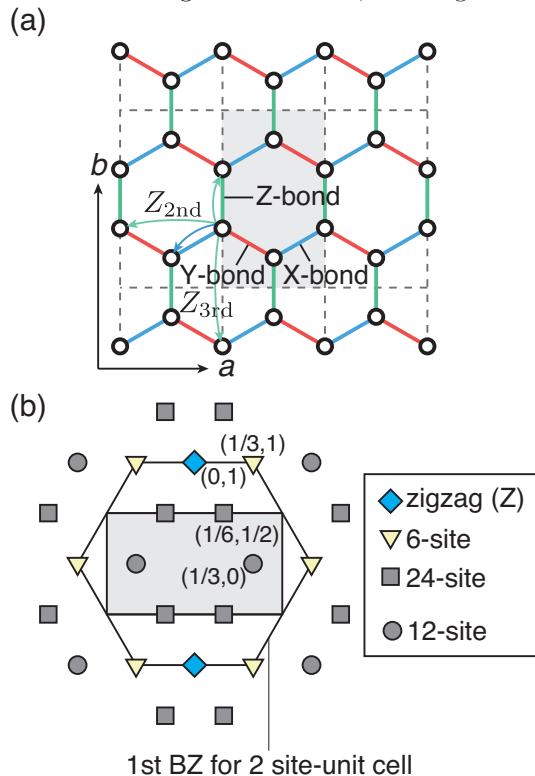


FIG. 6: (a) Experimental unit cell for honeycomb planes of iridium atoms. The horizontal and vertical axes represent the a - and b -axis of Na_2IrO_3 . The shaded rectangular area illustrates a unit cell consisting of 4 iridium atoms. The arrows illustrate the direction of the hoppings summarized in Table IV. (b) Peaks in spin structure factors calculated by using the Lanczos method for the 24-site cluster. The shaded rectangular area illustrates the 1st Brillouin zone (BZ) of Na_2IrO_3 . The hexagon represents the 1st Brillouin zone of the ideal honeycomb lattice whose unit cell contains two sites.

peak positions in the two-dimensional Brillouin zone are summarized.

However, anisotropy in alignments of ordered moments cannot be determined by the magnetic Bragg spots. Therefore we applied tiny local magnetic fields ($\sim 10^{-2}$ meV) to break symmetries and pin down the magnetic order pattern during the Lanczos steps. In Fig.2 and Fig.3 of the main article, normalized induced moments are illustrated.